High-Frequency Analysis of the Ellipticus Antenna

N. H. Younan, B. L. Cox, C. D. Taylor, and W. D. Prather

Abstract—**Efficient numerical solution techniques have been developed and used to examine the electromagnetic fields that can be developed in the working volume of the CW Ellipticus antenna operated at frequencies from 100 kHz to 1 GHz. An exponentially tapered transition section is designed to obtain the desired illumination pattern in the working volume. The input transition section is needed for impedance matching and to drive efficiently the Ellipticus antenna. A parametric study is performed to ascertain the performance of the Ellipticus antenna for frequencies up to 1 GHz.**

I. Introduction

Present EMP test facilities do not provide the required high-frequency illumination. Accordingly, a low-level continuous-wave (CW) facility, incorporating the Ellipticus antenna, is used to provide a horizontally polarized electric field to illuminate test objects [1], [2]. The original design specifications for the Ellipticus provided for an operating frequency range of 10 kHz to 100 MHz. Upgrading the Ellipticus CW antenna design to cover higher frequencies can be accomplished by using a transition section from the driver to the antenna that radiates up to a few gigahertz. This design is based on an exponentially tapered transmission line (ETTL) design that has radiator characteristics at high frequencies and serves as a matching section at low frequencies.

Due to the wide operating frequency range, a numerical rather than analytical analysis of the Ellipticus illuminator (EI) is required. A suitable procedure is developed that incorporates the NEC computer code [3]. Since the number of unknowns increases significantly with the frequency, a novel wire segmentation procedure is used [4]. This allows the analysis of very large wire configurations and provides sufficient accuracy with acceptable computer memory requirements and computational time.

In this paper, efficient numerical solution techniques have been developed to examine the electromagnetic fields that can be developed in the working volume of the Ellipticus facility operated at frequencies from approximately 100 kHz to 1 GHz. Moreover, a parametric study is performed to ascertain the performance of the Ellipticus illuminator for frequencies up to 1 GHz.

Manuscript received January 27, 1992; revised March 2, 1994.

N. H. Younan, B. L. Cox, and C. D. Taylor are with the Department of Electrical and Computer Engineering, Mississippi State University, Mississippi State, MS 39762 USA.

W. D. Prather is with Phillips Laboratory, Kirtland AFB, NM 87117 USA.

IEEE Log Number 9404483.

II. Description of the Ellipticus Illuminator

Fig. 1 shows the design structure of the CW Ellipticus antenna [5]. The Ellipticus antenna configuration is a distributed impedance loaded wire structure where the wire forms one half of an ellipse, cut along the semi-major axis, over a lossy ground. The antenna is 100 m across from the base and 20 m at its highest point, a very large structure in terms of a wavelength at a few gigahertz.

The structure is driven from its highest point, at the center, by a differential-mode CW driver thereby producing horizontal polarization of the electric field at the ground directly below the source. When a large object is illuminated, linear polarization is not expected over the entire surface. Typically, the test object is placed at the center of the Ellipticus antenna on the ground or raised off the ground on a rail car.

The antenna is constructed of 0.32-cm-diameter aircraft cable. The antenna is resistively loaded where the total antenna resistance is approximately 1750 Ω, placed 0.1 m apart along the length of the antenna.

III. NEC Modeling

A. Transition Section

The input transition section of the Ellipticus antenna for high-frequency applications is designed. The basic design is accomplished by using exponentially tapered transmission line analysis. Since transmission line theory does not account for radiation effects, the NEC code is then used to evaluate the design in terms of the input impedance and desired radiation pattern within the working volume. The input transition section is needed for impedance matching and to efficiently drive the Ellipticus antenna. The ETTL used to drive the EI structure of Fig. 1 is shown in Fig. 2. Details on the analysis and design of the exponentially tapered transmission line are given in [6].

Because of the large structure to be analyzed, the exponentially tapered transmission line of length l and driven by a 1-V source (Fig. 2) can be replaced by a Thevenin equivalent circuit for the

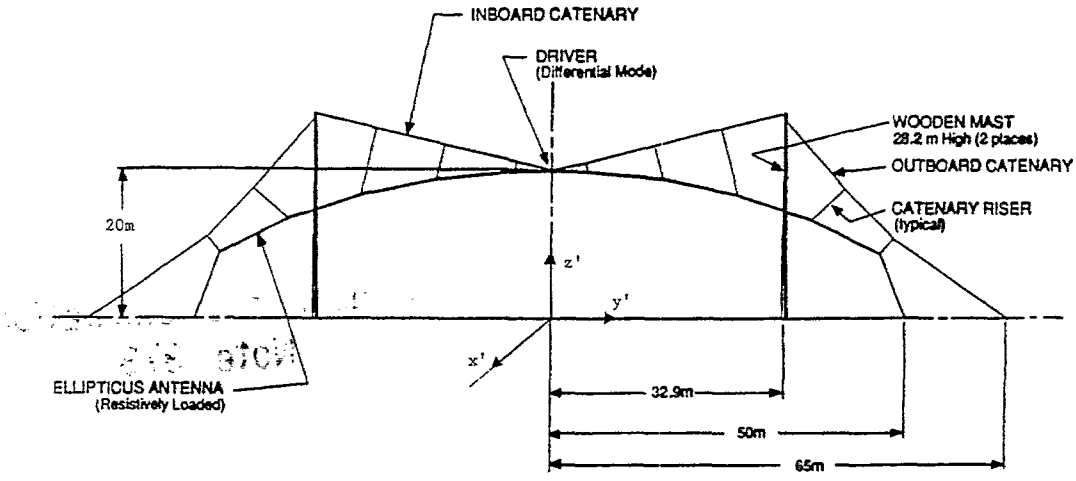

Fig. 1. The ellipticus illuminator structure.

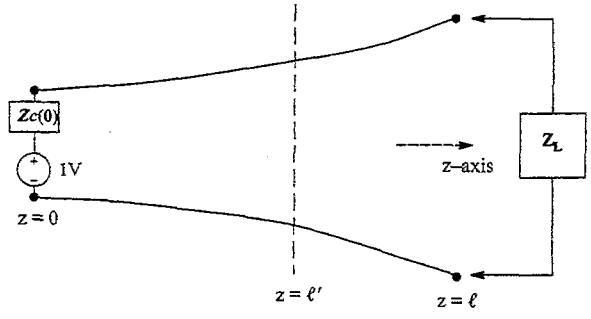

Fig. 2. The exponentially tapered transmission line (ETTL).

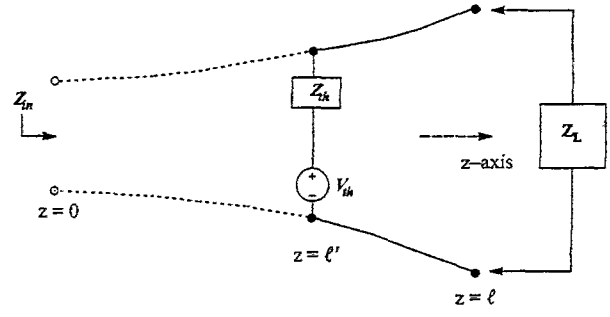

Fig. 3. Thevenin modeling of a portion of the ETTL.

portion from $z = 0$ to $z = l'$, $l' \leq l$, as shown in Fig. 3. This model is accurate to use in the NEC model as long as the wire spacing of the transmission line at $z = l'$ is much less than one wavelength.

The Thevenin equivalent model has $V_{\text{th}} = V_{\text{oc}}(l')$ and $Z_{\text{th}} = V_{\text{oc}}(l')/I_{\text{sc}}(l')$. Expressions for V_{th} and Z_{th} can be derived using the open-circuit and short-circuit conditions on the circuit of Fig. 3 [7]. The voltage and current on the exponentially tapered transmission line obey the following relationships [8]:

$$V(z) = V_1 e^{-\gamma_1' z} + V_2 e^{-\gamma_1'' z} \tag{1}$$

$$I(z) = \left(\frac{V_1 \gamma_1'}{j\omega L_0}\right) e^{-\gamma_2' z} + \left(\frac{V_2 \gamma_1''}{j\omega L_0}\right) e^{-\gamma_2'' z} \tag{2}$$

where

$$\gamma_{1,2}' = \mp \frac{q}{2} + j\beta \tag{3}$$

and

$$\gamma_{1,2}'' = \mp \frac{q}{2} - j\beta \tag{4}$$

with

$$\beta = \sqrt{\beta_0 - \left(\frac{q}{2}\right)^2}. \tag{5}$$

Here q is the taper factor and

$$\beta_0 = \omega\sqrt{L_0 C_0} = \frac{\omega L_0}{Z_c(0)} \tag{6}$$

where L_0 and C_0 are the inductance and capacitance per unit length at the input and $Z_c(0)$ is the input characteristic impedance.

Under open-circuit conditions, the voltage at $z = 0$ and the current at $z = l'$ can be expressed as

$$V(0) = 1 - I(0) Z_c(0) \tag{7}$$

and

$$I(l') = 0. \tag{8}$$

Evaluating (2) at $z = l'$ and equating it to (8) yields

$$\left(\frac{V_1 \gamma_1'}{j\omega L_0}\right) e^{-\gamma_2' l'} + \left(\frac{V_2 \gamma_1''}{j\omega L_0}\right) e^{-\gamma_2'' l'} = 0. \tag{9}$$

Similarly, evaluating (1) at $z = 0$ and equating it to (7) yields

$$V_1 + V_2 = 1 - \frac{Z_c(0)}{j\omega L_0}(V_1 \gamma_1' + V_2 \gamma_1''). \tag{10}$$

Solving for V_1 and V_2 yields

$$V_1 = \frac{j\beta_0 \gamma_1'' e^{-\gamma_2'' l'}}{\gamma_1'' e^{-\gamma_2'' l'}(\gamma_1' + j\beta_0) - \gamma_1' e^{-\gamma_2' l'}(\gamma_1'' + j\beta_0)} \tag{11}$$

and

$$V_2 = \frac{-j\beta_0 \gamma_1' e^{-\gamma_2' l'}}{\gamma_1'' e^{-\gamma_2'' l'}(\gamma_1' + j\beta_0) - \gamma_1' e^{-\gamma_2' l'}(\gamma_1'' + j\beta_0)}. \tag{12}$$

These expressions are then used in (1) with $z = l'$ to yield $V_{\text{th}} = V_{\text{oc}}(l')$, i.e.,

$$V_{\text{th}} = \frac{2\beta e^{ql'/2}}{\cos(\beta l')[2\beta + \tan(\beta l')(q + j2\beta_0)]}. \tag{13}$$

Under short-circuit conditions, (7) still holds and $V(l') = 0$. Evaluating (1) at $z = l'$ and using the fact that $V(l') = 0$ yields

$$V_1 e^{-\gamma_1' l'} + V_2 e^{-\gamma_1'' l'} = 0. \tag{14}$$

Solving for V_1 and V_2 yields

$$V_1 = \frac{j\beta_0 e^{-\gamma_1'' l'}}{e^{-\gamma_1'' l'}(\gamma_1' + j\beta_0) - e^{-\gamma_1' l'}(\gamma_1'' + j\beta_0)} \tag{15}$$

and

$$V_2 = \frac{-j\beta_0 e^{-\gamma_1' l'}}{e^{-\gamma_1'' l'}(\gamma_1' + j\beta_0) - e^{-\gamma_1' l'}(\gamma_1'' + j\beta_0)}. \tag{16}$$

These expressions are then used in (2) at $z = l'$ to yield $I_{sc}(l')$, i.e.,

$$I_{sc} = \frac{2\beta}{e^{ql'/2} Z_c(0)[2\beta \cos(\beta l') - q \sin(\beta l') + j2\beta_0 \sin(\beta l')]}. \tag{17}$$

Accordingly, Z_{th} is found to be

$$Z_{th} = Z_c(0)\, e^{ql'} \frac{2\beta - \tan(\beta l')[q - j2\beta_0]}{2\beta + \tan(\beta l')[q + j2\beta_0]}. \tag{18}$$

B. Ellipticus Illuminator Modeling

In the NEC modeling of the Ellipticus illuminator, the transition section is modeled by several straight-wire sections that approximate the curvature of the ETTL. However, due to the limitations of the wires spacing in the NEC program, the transition section is only modeled with straight wires up until the wire spacing approaches 4 or 5 wire radii in center-to-center separation. The remaining length of the transition section, denoted by l', is replaced by its Thevenin equivalent model of Fig. 3. Design parameters of $l = 1.935$ m, $Z_c(0) = 50\Omega$, and $Z_c(l) \approx 414\Omega$ are used throughout.

All of the EI except some or all of the transition section are modeled with straight wires. The coordinates for this wire model are taken from Fig. 1 for the main EI structure and from the tabulated values of the wire spacing used in the design of the ETTL [6]. These straight-wire approximations to the lower portion of the transition section are used for high frequencies, i.e., 100 MHz and up. For lower frequencies, the Thevenin equivalent circuit of Fig. 3 is used to model the entire transition section.

In addition to using the Thevenin equivalent circuit to model portions of the transition section, the EI is also modeled over a lossy ground plane. The Sommerfield/Norton method, SOMNEC, for analyzing wire structures near a lossy ground plane is used in the NEC computations. Accordingly, the parameters of the lossy ground plane are generated for each frequency used. The permittivity and conductivity values used are for concrete. These are obtained from data in a publication by Castillo and Singaraju [9]. Their constitutive parameter data are given only up to a frequency of 100 MHz. Accordingly, data extrapolation is performed to obtain approximate values of the parameters for higher frequencies, up to 1 GHz [10].

IV. Results

A. Input Impedance Calculation

The NEC modeling of the total structure, i.e., the Ellipticus Illuminator using the ETTL as a transition section gives the impedance seen by the voltage source used in the numerical model. These data are used along with the input impedance Z_{in} of the ETTL to compute the input impedance of the total structure at several frequencies of interest, where Z_{in} is given by [6]

$$Z_{in} = Z_c(0) \frac{Z_L[q \tan(\beta l) + 2\beta] + j2\beta_0 Z_c(0) e^{ql} \tan(\beta l)}{Z_c(0) e^{ql}[2\beta - q \tan(\beta l)] + j2Z_L\beta_0 \tan(\beta l)}. \tag{19}$$

Here, Z_L is the impedance of the main EI structure seen by the ETTL at $z = l$. Accordingly, the input impedance seen by looking into the total structure is obtained from the impedance seen by looking into the section that is modeled by the NEC code as transformed by the remaining portion of the ETTL (see Fig. 3).

In each case, Thevenin modeling of some or all of the ETTL transition section is used in the NEC model to determine the values of Z_L from which values of Z_{in} are found. Consequently, Z_L can be expressed as

$$Z_L = Z_{S\,NEC} - Z_{th} \tag{20}$$

where $Z_{S\,NEC}$ is the NEC source impedance seen by the driver source V_{th}.

In addition, the values for Z_L are adjusted to take into account the shunt inductance L of the source wire segment at high frequencies. Accordingly, Z_L is equal to Z_L as in (20) less a $j\omega L$ term, where L is given by [11]

$$\frac{L}{2x} = \frac{\mu_0}{2\pi}\left[\ln\left(\frac{2x}{a}\right) - 1 + \left(\frac{a}{x}\right) - 0.25\left(\frac{a}{x}\right)^2\right] \tag{21}$$

where x and a are the length and radius of the source wire segment, respectively.

For the lower frequencies cases, i.e., below 100 MHz, a length of $l' = l = 1.935$ m is used. This indicates that the entire ETTL transition section is being modeled with its Thevenin equivalent circuit. For higher frequencies, a length of $l' = 1.139$ m is used, i.e., the value of l' is equal to 1.935 m less the length of the portion modeled by straight-wire segments in the NEC model.

The resulting computed input impedances of the total structure are tabulated in Table I. At low frequencies, up to 26 MHz (cutoff frequency of the ETTL), the input impedance is dominated by the resistive loading of the Ellipticus structure. At higher frequencies, the input impedance of the structure begins to match the 50-Ω source impedance of the ETTL. This indicates that the ETTL behaves as a transmission line yielding VSWR values between 1.5 and 2 for most of the frequencies considered.

B. Incident Electric Field Computation

The incident electric field along the ground plane in the working volume is obtained via numerical modeling of the Ellipticus illuminator. The structure is modeled over a lossy ground plane using Thevenin equivalent circuit models for portions of the transition section. The resulting NEC code data obtained from these numerical modeling experiments consist of the total electric and magnetic fields along two lines in the working volume on the ground plane. Line (a) is defined at $x' = 6$ m, $y' = -15$ to 0 m, and $z' = 0$ m. On the other hand, line (b) is extended from $x' = 4.705$ to 7.295 m, with $y' = z' = 0$ m.

The incident field can be then approximated from the total electric and magnetic fields as follows [12]:

$$E_{x'}^{inc} \approx \tfrac{1}{2}[E_{x'}^{total} - (120\pi) H_{y'}^{total}] \tag{22}$$

and

$$E_{y'}^{inc} \approx \tfrac{1}{2}[E_{y'}^{total} + (120\pi) H_{x'}^{total}]. \tag{23}$$

These computations are performed for points 0.0625 m apart along line (a) and for points 0.01047 m apart along line (b). The magnitudes of the resulting incident-electric-field values are plotted to reveal the behavior of the incident field in this portion of the working volume.

Figs. 4 and 5 illustrate the dominant y component of the incident electric field at frequencies ranging from 100 kHz to 1 GHz along lines (a) and (b). As expected, field uniformity is achieved within the working volume of the Ellipticus antenna. In addition, some oscillatory variations in the principal component of the electric field occur within the plane of the Ellipticus antenna as seen in Fig. 4.

TABLE I
CALCULATED INPUT IMPEDANCES OF THE TOTAL STRUCTURE USING THE RESULTS OBTAINED FROM THE NEC-2 MODELING AT VARIOUS FREQUENCIES

FREQUENCY (MHz)	INPUT IMPEDANCE (Ω)	VSWR
0.1	1848.6 - j 49.2	37.0
0.2	1829.0 - j 130.7	36.8
0.3	1858.3 - j 254.9	37.9
0.4	1868.6 - j 412.1	39.2
0.5	1842.4 - j 631.8	41.2
0.6	1774.8 - j 816.3	43.0
0.7	1626.8 - j 991.1	44.6
0.8	1424.3 - j1122.0	46.2
0.9	1228.7 - j1206.5	48.3
1	1029.9 - j1211.8	49.1
5	204.0 - j 365.2	17.3
10	78.7 - j 236.7	16.4
100	49.8 - j 23.1	1.6
200	45.8 + j 5.1	1.1
300	43.2 - j 11.8	1.3
500	75.2 - j 1.6	1.5
800	41.0 - j 17.1	1.5
1000	53.8 + j 25.8	1.6

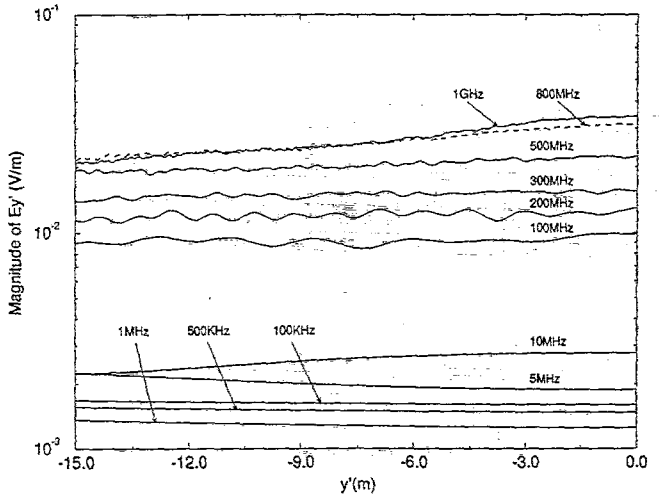

Fig. 4. Incident E-field along line $x' = 6$ m and $z' = 0$ m.

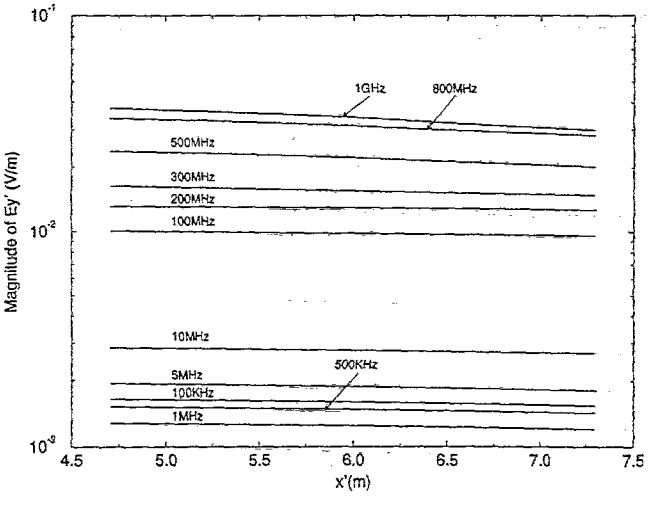

Fig. 5. Incident E-field along line $y' = 0$ m and $z' = 0$ m.

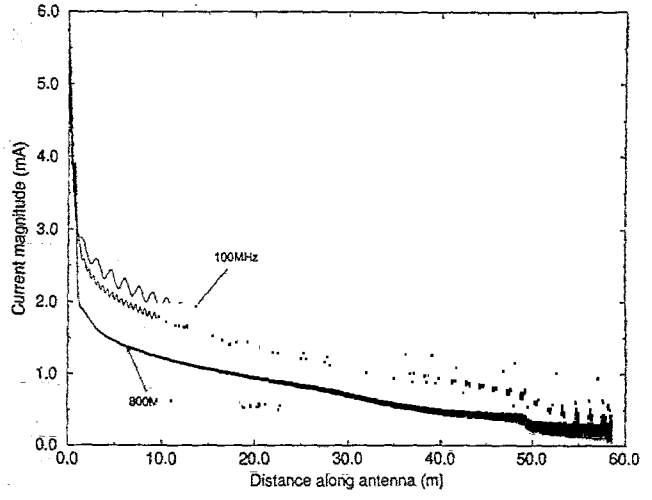

Fig. 6. Currents on half the ellipticus structure at 800, 300, and 100 MHz.

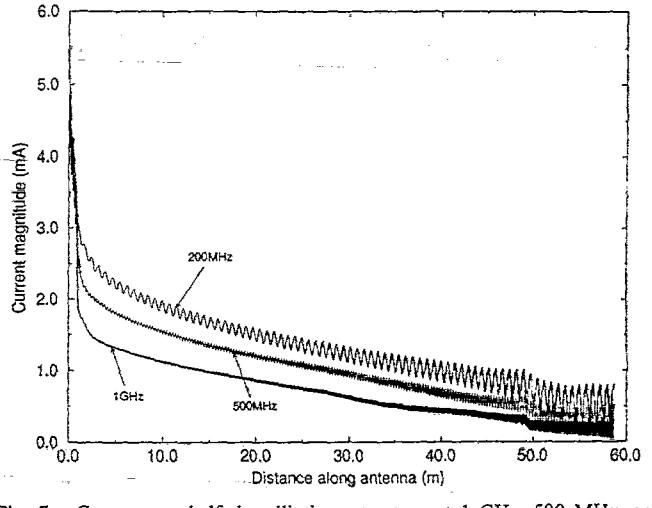

Fig. 7. Currents on half the ellipticus structure at 1 GHz, 500 MHz, and 200 MHz.

This must be the result of the oscillatory variations in the antenna current with distance from the source. Along the line perpendicular to the plane of the antenna, there is no oscillatory behavior as seen in Fig. 5. This is expected since the points along line (b) maintain a constant relative separation from the antenna currents.

C. Current Computation

The NEC modeling of the Ellipticus antenna also yields the computed currents on the structure at different frequencies, ranging from 100 kHz to 1 GHz. Figs. 6–9 illustrate the resulting current along the structure with the presence of the transition section. The junction

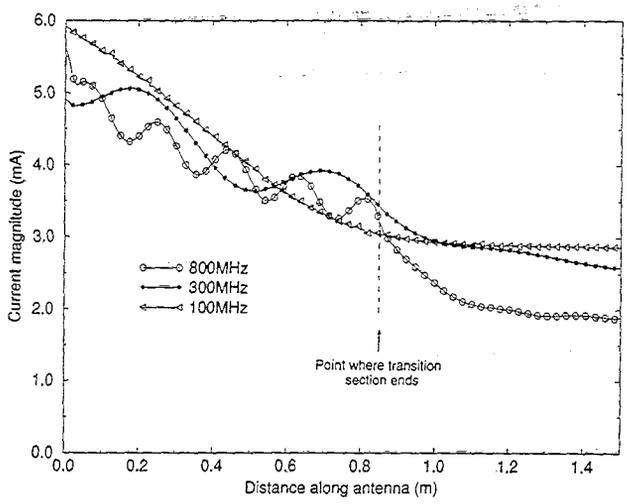

Fig. 8. Currents in the transition section at 800, 300, and 100 MHz.

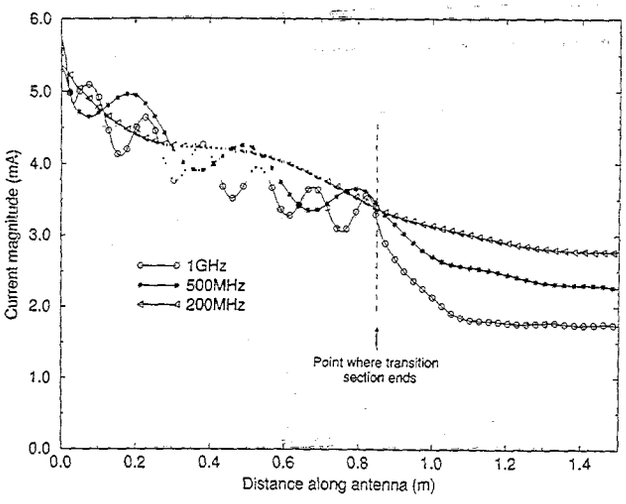

Fig. 9. Currents in the transition section at 1 GHz, 500 MHz, and 200 MHz.

of the main EI structure with the transition section is indicated by a dashed line, where the length of the transition section lies from the origin to the dashed line. Moreover, details of the current within the transition section are also shown to better analyze the behavior of the Ellipticus antenna. Clearly, the wire current magnitude decreases rapidly with distance from the driving point (origin) at high frequencies. In addition, the current in the transition section has a standing-wave behavior at high frequencies, with about a half-wavelength separation between any two peaks or two minima and with VSWR values of approximately 1.5. This is consistent with the results shown in Table I.

V. Conclusion

Numerical techniques have been utilized to examine the electromagnetic fields that can be developed in the working volume of the CW Ellipticus antenna operated at frequencies ranging from approximately 100 kHz to 1 GHz with an exponentially tapered input section. The NEC code is used to analyze the Ellipticus configuration with the transition section present. The input transition section is needed for impedance matching and to drive efficiently the Ellipticus antenna. Calculations from the NEC code indicate that field uniformity is achieved within the working volume of the Ellipticus antenna. Moreover, the current in the transition section exhibits a standing-wave behavior at high frequencies consistent with impedance calculations. These results indicate that the transition section design, based on the exponentially tapered transmission line, performs as an impedance-matching element. This provides an increased bandwidth for operating the Ellipticus antenna.

References

[1] W. D. Prather and C. E. Baum, "Elliptic CW antenna design," Miscellaneous Simulator Memos, Memo 22, Mar. 1987.
[2] C. Zuffada, F. C. Yang, and I. Wong, "On the thin toroidal and elliptical antennas," BDM Corp. Sensor and Simulation Notes, Note 315, Jan. 1989.
[3] G. J. Burke and A. J. Poggio, "Numerical electromagnetics code (NEC) method of moments," Naval Ocean Systems Center Tech. Rep. NOSCTSD 116, Jan. 1981.
[4] S. N. Tabet, J. P. Donohoe, and C. D. Taylor, "Using nonuniform segment lengths with NEC to analyze electrically long wire antenna," *ACES J.*, vol. 5, no. 2, pp. 2–16, Winter 1990.
[5] T. Dana, "Ellipticus CW antenna system as built drawings," U.I.E. Tech. Rep. TR-89-0026, Dec. 1989.
[6] N. H. Younan and B. L. Cox, "GigaHertz analysis of the ellipticus antenna," BDM Corp., Sensor and Simulation Notes, Note 325, Apr. 1991.
[7] C. W. Harrison, Jr., "Folded wire structures as receiving antennas," Tech. Memo. SCTM 253-58-(14), Sandia Corp., June 1958.
[8] S. Ramo, J. R. Whinnery, and T. Van Duzer, *Fields and Waves in Communication Electronics* New York: Wiley, 1965.
[9] J. P. Castillo and B. K. Singaraju, "Effects of wave reflection on objects near a plane ground," *Athamas Memos*, memo 8, May 1975.
[10] J. P. Donohoe and S. N. Tabet, "HSI high frequency performance verification upgrade," Final Rep. Contract No. F29601-88-C-0001, Subtask 03-05/00, Nov. 1989.
[11] E. C. Jordan and K. G. Balmain, *Electromagnetic Waves and Radiating Systems*. Englewood Cliffs, NJ: Prentice-Hall, 1968.
[12] E. G. Farr, "Extrapolation of ground-alert mode data at hybrid EMP simulators," BDM Corp., Sensor and Simulation Notes, Note 311, July 1988.